# SCATTERING FROM THREE-DIMENSIONAL DISPERSIVE GYROTROPIC BODIES USING THE TLM METHOD

**A. F. Yagli**

Konya Yolu 40.km Golbasi
Ankara, Turkey

**J. K. Lee and E. Arvas**

Department of Electrical Engineering and Computer Science
Syracuse University
Syracuse, NY 13244, USA

**Abstract**—A three-dimensional scattering field Transmission Line Modeling (TLM) algorithm is established to obtain bistatic radar cross sections of frequency dispersive gyromagnetic objects. Starting from the 1D TLM modeling of gyrotropic materials, a scattering field TLM algorithm is derived for 3D calculations. For verification, the bistatic radar cross section results for several gyromagnetic structures are compared with the single frequency computations, where the permittivity and permeability tensors are made of complex constants at a given frequency.

## 1. INTRODUCTION

Electromagnetic modeling of anisotropic materials has been a hot research topic. Because of its unique properties, gyrotropic medium has attracted the interest of the researchers. Gyrotropic materials are widely used in circulators, cavities and similar waveguide devices. The polarization rotation property of these materials makes them a research area for optical applications, too. The finite difference time domain (FDTD) analysis of magnetized plasma was first done by Hunsberger et al. [1], where they used discrete convolution in order to model the frequency dependency of the material. Hunsberger also modeled magnetized ferrite and chiral materials using the same

---
Corresponding author: A. F. Yagli (afyagli@gmail.com).

technique [2]. The examples he solved were one dimensional gyrotropic slab problems of which the reflection and transmission coefficients were obtained.

The Transmission Line Modeling (TLM) method is a robust and efficient numerical technique to model electromagnetic problems in time domain. Hybrid Symmetrical Condensed Node approach of TLM method was used by Yaich et al. to model the magnetized plasma slab problem [3] and the magnetized ferrite slab problem [4]. On the other hand, Paul used TLM method to model gyrotropic materials, where he introduced a different approach using $Z$ transform in order to adapt the frequency dependency of the media to discrete time domain [5]. The $Z$ transform is most widely used of the functional transformations of sequences (i.e., discrete time domain signals) in the theory of discrete signals and systems [6]. The implementation of $Z$ transform in FDTD analysis of frequency dependent media was first introduced by Sullivan [7–9]. Huang and Li used FDTD analysis with $Z$ transformation to model the electromagnetic propagation in a magnetized plasma, and showed that the $Z$ transform algorithm is more accurate than the recursive convolution algorithm [10].

In this paper, a scattering field TLM algorithm is derived to calculate the electromagnetic scattering of three dimensional frequency dispersive gyrotropic objects. With the help of the 1D TLM modeling of gyrotropic materials by Paul [5, 11], a scattering field TLM algorithm is derived for 3D calculations. The bistatic radar cross section results of the gyromagnetic structures are obtained from the simulations and compared with our monochromatic calculations at some frequencies where the diagonal susceptibility tensor elements have real non-negative values [12–14].

Since our TLM computation space is truncated, a near field to far field transformation method is also used to obtain the far field scattering [15, 16]. The incident field for our frequency dispersive algorithm is chosen to be a Gaussian wave, and the bistatic RCS values for the desired frequency are calculated using the discrete Fourier transform.

## 2. TLM MODELING OF 3D FREQUENCY DISPERSIVE GYROTROPIC OBJECTS

For TLM modeling of anisotropic 3D materials, we modified Paul's TLM algorithm [5, 11] to a scattering field formulation. Assuming the conductivity tensors to be zero, in Paul's TLM algorithm the relation between the port excitations ($\overline{F}^e$) and the field quantities ($\overline{F}$) is given

in Laplace domain as

$$2\overline{F}^e = 4\overline{F} + 2s\Delta t\overline{\overline{M}}\,\overline{F} \tag{1}$$

In scattering field formulation this equation becomes

$$2\overline{F}^e_{scat} = 4\overline{F}_{scat} + 2s\Delta t\overline{\overline{M}}\,\overline{F}_{scat} + 2s\Delta t\overline{\overline{M}}\,\overline{F}_{inc} \tag{2}$$

where $s = j2\pi f$ and $\overline{F} = \overline{F}_{scat} + \overline{F}_{inc}$; $\overline{F}_{scat}$ and $\overline{F}_{inc}$ are the normalized scattered and incident field vectors as we discussed in [13]. $\overline{F}$ is the field vector which has the voltage and current values of the TLM cell described by Paul [5]. We introduce

$$\overline{F}_{inc} = \begin{bmatrix} V_x^{inc} \\ V_y^{inc} \\ V_z^{inc} \\ i_x^{inc} \\ i_y^{inc} \\ i_z^{inc} \end{bmatrix} \tag{3}$$

$$\overline{F}_{scat} = \begin{bmatrix} V_x^{scat} \\ V_y^{scat} \\ V_z^{scat} \\ i_x^{scat} \\ i_y^{scat} \\ i_z^{scat} \end{bmatrix} \tag{4}$$

In (2), $\overline{\overline{M}}$ is the general material tensor which describes dielectric and magnetic properties. The discrete time domain model is obtained from (2) using bilinear $Z$ transform, where $s\Delta t$ is replaced with

$$s\Delta t = 2\frac{1 - z^{-1}}{1 + z^{-1}} \tag{5}$$

We use the partial fraction expansions as

$$\left(1 - z^{-1}\right)\overline{\overline{M}}(z) = \overline{\overline{M}}_0 + z^{-1}\left(\overline{\overline{M}}_1 + \overline{\overline{M}}_2(z)\right) \tag{6}$$

which leads us to

$$
\begin{aligned}
&\overline{\overline{T}}^{-1}\,\overline{F}_{scat} \\
&= 2\overline{F}^e_{scat} - 4\overline{\overline{M}}_0\overline{F}_{inc} \\
&\quad + z^{-1}\left(2\overline{F}^e_{scat} + \overline{\overline{\kappa}}\,\overline{F}_{scat} - 4\overline{\overline{M}}_1\,\overline{F}_{inc} - 4\overline{\overline{M}}_2(z)\left(\overline{F}_{scat} + \overline{F}_{inc}\right)\right)
\end{aligned} \tag{7}
$$

where

$$\overline{\overline{T}}^{-1} = 4\overline{\overline{I}} + 4\overline{\overline{M}}_0 \tag{8}$$

and

$$\overline{\overline{\kappa}} = -4\overline{\overline{I}} - 4\overline{\overline{M}}_1. \tag{9}$$

The tensor $\overline{\overline{M}}_2$ is a function of $z$, while $\overline{\overline{M}}_0$ and $\overline{\overline{M}}_1$ are constant parameter tensors. (7) can be rewritten as

$$\overline{F}_{scat} = \overline{\overline{T}} \left( 2\overline{F}^e_{scat} - 4\overline{\overline{M}}_0 \overline{F}_{inc} + z^{-1}\overline{S} \right) \tag{10}$$

Or in time domain representation,

$$\overline{F}_{scat}[n] = \overline{\overline{T}} \left( 2\overline{F}^e_{scat}[n] - 4\overline{\overline{M}}_0 \overline{F}_{inc}[n] + \overline{S}[n-1] \right) \tag{11}$$

with time index $n$.

## 2.1. Gyromagnetic Objects

Gyromagnetic materials are represented by a permeability tensor and a scalar permittivity value. We are going to use a permittivity of $\varepsilon_0$ (permittivity of free space) for our magnetized ferrite material. Since longitudinal propagation will be modeled in this section, we will assume a relative permeability tensor of

$$\overline{\overline{\mu}} = \begin{bmatrix} \mu_1 & j\mu_2 & 0 \\ -j\mu_2 & \mu_1 & 0 \\ 0 & 0 & \mu_3 \end{bmatrix} \tag{12}$$

where the applied magnetic field is in $z$ direction (i.e., $\overline{H}_0 = \hat{z}H_0$) in Cartesian coordinates. The tensor elements are given as [1, 17]

$$\mu_1 = 1 + \frac{(\omega_0 + j\omega\alpha)\omega_m}{(\omega_0 + j\omega\alpha)^2 - \omega^2} = 1 + \chi_1 \tag{13}$$

$$\mu_2 = \frac{\omega\omega_m}{(\omega_0 + j\omega\alpha)^2 - \omega^2} = \frac{\chi_2}{j} \tag{14}$$

$$\mu_3 = 1 = 1 + \chi_3 \tag{15}$$

where $\alpha$ is the damping factor, $\omega_m$ is the saturation magnetization frequency, and $\omega_0$ is the Larmor precessional frequency.

The magnetic susceptibilities are

$$\overline{\overline{\chi}}_m = \begin{bmatrix} \chi_m^{xx} & \chi_m^{xy} & 0 \\ \chi_m^{yx} & \chi_m^{yy} & 0 \\ 0 & 0 & \chi_m^{zz} \end{bmatrix} = \begin{bmatrix} \chi_1 & \chi_2 & 0 \\ -\chi_2 & \chi_1 & 0 \\ 0 & 0 & \chi_3 \end{bmatrix} \tag{16}$$

In order to assemble these susceptibility tensors into our TLM algorithm, we have to first transform these frequency dependent functions into Laplace domain, from which we can easily move to $Z$ domain.

$\chi_1$ can be written in Laplace domain as

$$\chi_1(s) = \frac{(\omega_0 + s\alpha)\omega_m}{(\omega_0 + s\alpha)^2 + s^2} \tag{17}$$

which can be rewritten as

$$\chi_1(s) = \omega_m \Re \left[ \frac{-j}{s - j(\omega_0 + s\alpha)} \right] \tag{18}$$

where the operator $\Re[.]$ implies the real part of $[.]$. If we call $\tau_m = \dfrac{1 - j\alpha}{-j\omega_0}$, and $\tau_a = \dfrac{1}{1 - j\alpha}$, (18) will have the form of

$$\chi_1(s) = \omega_m \Re \left[ \tau_a \frac{-j\tau_m}{1 + s\tau_m} \right] \tag{19}$$

Similarly, $\chi_2$ can be formulated in Laplace domain as

$$\chi_2(s) = \frac{s\omega_m}{(\omega_0 + s\alpha)^2 + s^2} \tag{20}$$

and in another form

$$\chi_2(s) = \omega_m \Re \left[ \frac{1}{s - j(\omega_0 + s\alpha)} \right] \tag{21}$$

or

$$\chi_2(s) = \omega_m \Re \left[ \tau_a \frac{\tau_m}{1 + s\tau_m} \right] \tag{22}$$

Transforming Laplace domain equations to $Z$ domain we use

$$\frac{\tau_m}{1 + s\tau_m} \rightarrow \frac{\tau_m}{1 + \frac{2(1 - z^{-1})}{\Delta t(1 + z^{-1})}\tau_m} \tag{23}$$

In order to have a similar form as in (6), we will multiply right hand side of the equation above by $(1 - z^{-1})$ and use partial fraction expansion.

$$\left(1 - z^{-1}\right) \frac{\tau_m}{1 + \frac{2(1 - z^{-1})}{\Delta t(1 + z^{-1})}\tau_m}$$

$$= \frac{\tau_m \Delta t}{2\tau_m + \Delta t}$$

$$+ z^{-1} \left[ \frac{\tau_m \Delta t(2\tau_m - \Delta t)}{(2\tau_m + \Delta t)^2} - \frac{z^{-1}\frac{8\tau_m^2 \Delta t^2}{(2\tau_m + \Delta t)^3}}{1 - z^{-1}\frac{2\tau_m - \Delta t}{2\tau_m + \Delta t}} \right]$$

$$= \beta_0 + z^{-1}(\beta_1 + \beta_2) \tag{24}$$

We only have $\beta_2$ as a function of $z$.

$$\beta_2 = \frac{z^{-1}\frac{-8\tau_m^2\Delta t^2}{(2\tau_m+\Delta t)^3}}{1 - z^{-1}\frac{2\tau_m-\Delta t}{2\tau_m+\Delta t}} = \frac{z^{-1}b_1}{1 - z^{-1}a_1} \tag{25}$$

When we are transforming $\chi_2(s)$ to $Z$ domain, we can use the equations above. On the other hand, for transformation of $\chi_1(s)$ to $Z$ domain, all $\beta$ terms should be multiplied by $-j$. Then we can formulate $(1-z^{-1})\chi_1$ in $Z$ domain as

$$\left(1 - z^{-1}\right)\chi_1(z) = \omega_m\Re\left[-j\tau_a\left(\beta_0 + z^{-1}\left(\beta_1 + \beta_2\right)\right)\right] \tag{26}$$

And $(1 - z^{-1})\chi_2$ will be

$$\left(1 - z^{-1}\right)\chi_2(z) = \omega_m\Re\left[\tau_a\left(\beta_0 + z^{-1}\left(\beta_1 + \beta_2\right)\right)\right] \tag{27}$$

(26) and (27) can be rewritten as

$$\left(1 - z^{-1}\right)\chi_1(z) = \chi_{10} + z^{-1}(\chi_{11} + \chi_{12}(z)) \tag{28}$$

$$\left(1 - z^{-1}\right)\chi_2(z) = \chi_{20} + z^{-1}(\chi_{21} + \chi_{22}(z)) \tag{29}$$

Thus, we can build our $\overline{\overline{M}}$ matrices in the following forms

$$\overline{\overline{M}}_0 = \begin{bmatrix} 0 & 0 & 0 & 0 & 0 & 0 \\ 0 & 0 & 0 & 0 & 0 & 0 \\ 0 & 0 & 0 & 0 & 0 & 0 \\ 0 & 0 & 0 & \chi_{10} & \chi_{20} & 0 \\ 0 & 0 & 0 & -\chi_{20} & \chi_{10} & 0 \\ 0 & 0 & 0 & 0 & 0 & 0 \end{bmatrix},$$

$$\overline{\overline{M}}_1 = \begin{bmatrix} 0 & 0 & 0 & 0 & 0 & 0 \\ 0 & 0 & 0 & 0 & 0 & 0 \\ 0 & 0 & 0 & 0 & 0 & 0 \\ 0 & 0 & 0 & \chi_{11} & \chi_{21} & 0 \\ 0 & 0 & 0 & -\chi_{21} & \chi_{11} & 0 \\ 0 & 0 & 0 & 0 & 0 & 0 \end{bmatrix}, \tag{30}$$

$$\overline{\overline{M}}_2 = \begin{bmatrix} 0 & 0 & 0 & 0 & 0 & 0 \\ 0 & 0 & 0 & 0 & 0 & 0 \\ 0 & 0 & 0 & 0 & 0 & 0 \\ 0 & 0 & 0 & \chi_{12} & \chi_{22} & 0 \\ 0 & 0 & 0 & -\chi_{22} & \chi_{12} & 0 \\ 0 & 0 & 0 & 0 & 0 & 0 \end{bmatrix}$$

In our 3D anisotropic TLM algorithm, we can use $\overline{\overline{M}}_0$, $\overline{\overline{M}}_1$ and $\overline{\overline{M}}_2$ in Equation (7).

We defined a discrete time step state vector $\overline{S}$ in (10) as

$$\overline{S} = 2\overline{F}^e_{scat} + \overline{\overline{\kappa}} \, \overline{F}_{scat} - 4\overline{\overline{M}}_1 \, \overline{F}_{inc} - 4\overline{\overline{M}}_2(z) \left( \overline{F}_{scat} + \overline{F}_{inc} \right) \quad (31)$$

Let $\overline{S}_m = \overline{\overline{M}}_2(z)(\overline{F}_{scat} + \overline{F}_{inc})$. $\overline{S}_m$ vector has the form of

$$\overline{S}_m = \begin{bmatrix} 0 \\ 0 \\ 0 \\ \Re[S_{m4}] \\ \Re[S_{m5}] \\ 0 \end{bmatrix} \quad (32)$$

We will develop the forth element of $\overline{S}_m$ (i.e., $\Re[S_{m4}]$) due to the elements of field vector $\overline{F}$, which are $i_x$ ($i_x = i_x^{scat} + i_x^{inc}$) and $i_y$ ($i_y = i_y^{scat} + i_y^{inc}$).

$$S_{m4} = \omega_m \tau_a \left( -j\beta_2 i_x + \beta_2 i_y \right) \quad (33)$$

When we place the open form of $\beta_2$ in (33), we have

$$S_{m4} = \omega_m \tau_a \left( -j \frac{z^{-1}b_1}{1 - z^{-1}a_1} i_x + \frac{z^{-1}b_1}{1 - z^{-1}a_1} i_y \right) \quad (34)$$

$$\left( 1 - z^{-1}a_1 \right) S_{m4} = \omega_m \tau_a \left( -jz^{-1}b_1 i_x + z^{-1}b_1 i_y \right) \quad (35)$$

$$S_{m4} = \omega_m \tau_a \left( -jz^{-1}b_1 i_x + z^{-1}b_1 i_y \right) + z^{-1}a_1 S_{m4} \quad (36)$$

In time domain representation, the iterative update of $S_{m4}$

$$\begin{aligned} S_{m4}[n] &= \omega_m \tau_a \left( -jb_1 \left( i_x^{scat}[n-1] + i_x^{inc}[n-1] \right) + b_1 \left( i_y^{scat}[n-1] + i_y^{inc}[n-1] \right) \right) \\ &\quad + a_1 S_{m4}[n-1] \end{aligned} \quad (37)$$

where $n$ is the discrete time index.

Similarly, the calculation of the fifth element of the vector $\overline{S}_m$ (i.e., $\Re[S_{m5}]$) can be formulated as

$$S_{m5} = \omega_m \tau_a \left( -jz^{-1}b_1 i_y - z^{-1}b_1 i_x \right) + z^{-1}a_1 S_{m5} \quad (38)$$

and in time domain

$$\begin{aligned} S_{m5}[n] &= \omega_m \tau_a \left( -jb_1 \left( i_y^{scat}[n-1] + i_y^{inc}[n-1] \right) - b_1 \left( i_x^{scat}[n-1] + i_x^{inc}[n-1] \right) \right) \\ &\quad + a_1 S_{m5}[n-1] \end{aligned} \quad (39)$$

Updating the new field values is followed by determining the reflected port voltages as described by Paul [11]. The TLM computation process will continue with sending these reflected port

voltages to the neighboring cells as their new incident port voltages for
the next time step.

   In our simulations we used a Gaussian wave as the incident wave
propagating in $z$ direction, which has electric field component in $x$
direction. The $\overline{F}_{inc}$ vector has the form of

$$\overline{F}_{inc} = \begin{bmatrix} V_{inc} \\ 0 \\ 0 \\ 0 \\ i_{inc} \\ 0 \end{bmatrix} \tag{40}$$

where

$$V_{inc} = i_{inc} = -\Delta l \; e^{-A\left(\Delta t(n-n_0)-\frac{\Delta l}{c}(z-z_0)\right)^2} \tag{41}$$

$n$ is the time step index and $z$ is the $z$ coordinate index of the cell.
We have $-\Delta l$ in the front, since these quantities are normalized fields.
$V_{inc}$ is in the first row, which denotes the E field in $x$ direction, while
$i_{inc}$ is in the fifth row to represent the H field in $y$ direction. $A$ is the
constant that determines the width of the pulse, while $n_0$ and $z_0$ are
delays in time and space, respectively.

   The incident fields are injected to the simulation domain
analytically and the electric and magnetic surface currents due
to scattering fields on the imaginary closed surface enclosing the
gyrotropic structure are stored for each time step. Then the far field
RCS data is generated using these surface currents. The TLM cell
parameters are different than Paul's total field parameters. Incident
and reflected port voltages of the 12 ports of a TLM cell are transferring
only the scattering field information to the neighboring cells in our
algorithm. The port voltage values of a cell are updated according to
the scattering field information coming from the neighboring cells and
the analytically injected incident field to that specific cell. The scheme
of transferring the port voltages between the neighboring cells is the
same as that of Paul. Using this method we can easily generate any
form of incident field on any 3D arbitrarily shaped structure.

## 3. RADAR CROSS SECTIONS OF 3D GYROMAGNETIC OBJECTS

In order to demonstrate the algorithm we developed in this paper,
we used our single frequency 3D formulation [13] to compare our new
results. In [13], the scattering of a ferrite sphere is compared with the
bistatic RCS of the same sphere in the study of Geng et al. [18]. The
monochromatic 3D formulation is easier to derive since $\overline{\overline{M}}$ matrix has

constant valued elements, which does not force the algorithm to have a complex update scheme. In monochromatic formulation we can obtain one RCS result for one simulation at a given frequency. On the other hand, using the frequency dispersive formula, one can get RCS results for multiple frequencies in one simulation.

To model, we have chosen three gyromagnetic structures — sphere, cube and finite cylinder — with material parameters, $\omega_0 = 2\pi 20 \times 10^9$ [rad/s] as the Larmor precessional frequency, $\omega_m = 2\pi 20 \times 10^9$ [rad/s] as the saturation magnetization frequency and $\alpha = 0.1$ as the damping factor. The real and imaginary parts of the relative permeability tensor elements are given in Figure 1. The tensor element values for single frequency simulations are calculated using the frequency dependent formulations of the relative permeability tensor elements. We ran our single frequency simulations at 7 GHz, 8 GHz, 9 GHz and 10 GHz.

Using the time domain we obtain the response of the material for a wide band of frequency. But we have to verify our frequency dispersive RCS results. Since we could not manage to find any study showing time domain solution for 3D RCS results of frequency dispersive gyrotropic materials in the literature, we developed SF method to obtain the RCS of the same structure at a given frequency [13]. But single frequency method only works for the media where the permittivity or permeability tensor should have non-negative number for the real part of the complex diagonal element. We had chosen these four frequencies, because the real parts of the complex numbers on the diagonal sections of the permeability tensors are non-negative.
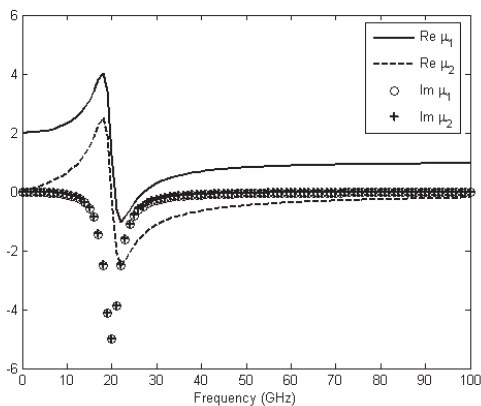


**Figure 1.** The real and imaginary parts of the relative permeability tensor elements of the magnetized ferrite.

For 7 GHz, the tensor has the form of

$$\overline{\overline{\mu}} = \begin{bmatrix} 2.137 - j0.05 & j(0.397 - j0.032) & 0 \\ -j(0.397 - j0.032) & 2.137 - j0.05 & 0 \\ 0 & 0 & 1 \end{bmatrix} \quad (42)$$

At 8 GHz, we have the relative permeability tensor of

$$\overline{\overline{\mu}} = \begin{bmatrix} 2.185 - j0.065 & j(0.472 - j0.045) & 0 \\ -j(0.472 - j0.045) & 2.185 - j0.065 & 0 \\ 0 & 0 & 1 \end{bmatrix} \quad (43)$$

and for 9 GHz, we have

$$\overline{\overline{\mu}} = \begin{bmatrix} 2.247 - j0.085 & j(0.558 - j0.063) & 0 \\ -j(0.558 - j0.063) & 2.247 - j0.085 & 0 \\ 0 & 0 & 1 \end{bmatrix} \quad (44)$$

For 10 GHz, the tensor becomes

$$\overline{\overline{\mu}} = \begin{bmatrix} 2.323 - j0.11 & j(0.656 - j0.088) & 0 \\ -j(0.656 - j0.088) & 2.323 - j0.11 & 0 \\ 0 & 0 & 1 \end{bmatrix} \quad (45)$$

In modeling of the gyromagnetic sphere, the diameter is taken as 33.4 mm, while the space discretization is $\Delta l = 1.67$ mm. The diameter of the sphere is chosen to have one wavelength at around 9 GHz. In order to ensure the accuracy, the cell size is set to $\lambda/20$. The time step value becomes $\Delta t = 2.78$ psec.

In the frequency dispersive formulation, the incident field is chosen as a Gaussian wave form. We waited until the fields reach the steady state. We first consider the wave incident on a gyromagnetic sphere in free space as shown in Figure 2.
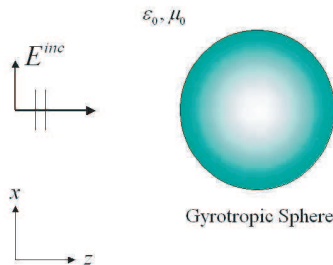


**Figure 2.** Incidence of a plane wave on a gyrotropic sphere in free space.

The bistatic RCS calculations of frequency dispersive (FD) and single frequency (SF) computations for a sphere case are given in Figures 3 to 6 at four different frequencies. The results show fairly good agreement. Since we discretize both time and space, the tensor elements we take for single frequency computations change, which results in some discrepancy. Finer mesh will give better solutions.
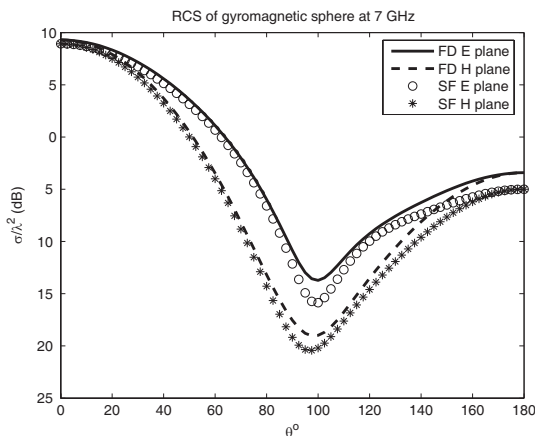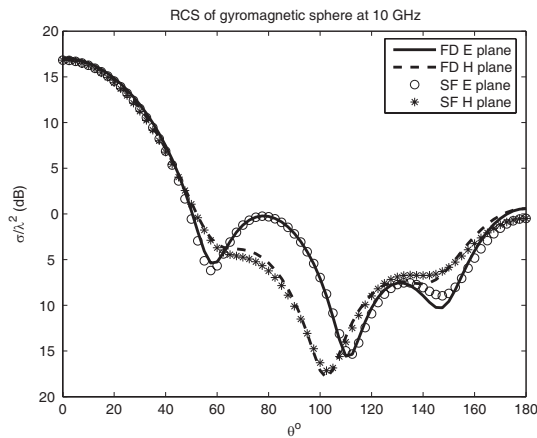


**Figure 3.** The bistatic RCS of frequency dispersive and single frequency simulations of the gyromagnetic sphere at 7 GHz.
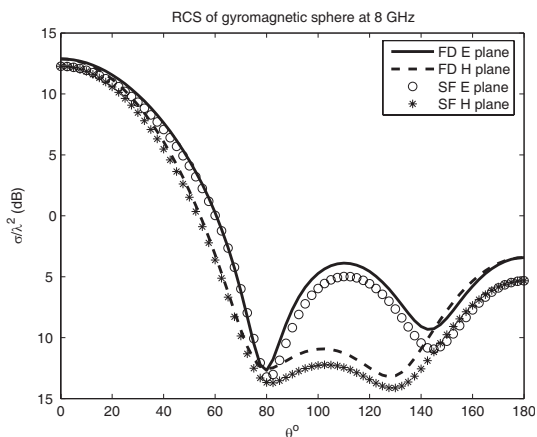


**Figure 4.** The bistatic RCS of frequency dispersive and single frequency simulations of the gyromagnetic sphere at 8 GHz.
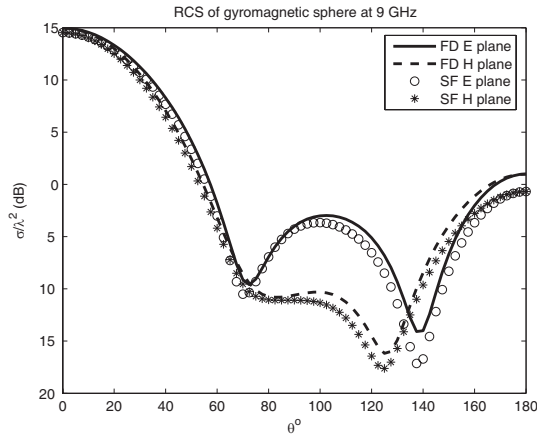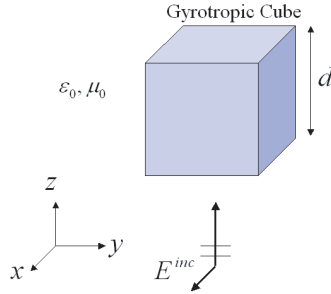
**Figure 5.** The bistatic RCS of frequency dispersive and single frequency simulations of the gyromagnetic sphere at 9 GHz.



**Figure 6.** The bistatic RCS of frequency dispersive and single frequency simulations of the gyromagnetic sphere at 10 GHz.

In the figures, $\theta$ is the observation angle in spherical coordinates. $\theta = 0°$ is the $+z$ direction, while $\theta = 180°$ is $-z$ direction which is the backscattering observation angle.

Next we consider the wave incident on a gyromagnetic cube (Figure 7). The space and time discretization values are kept the same as in the sphere case. The length of one edge of the cube is chosen to be $d = 33.4$ mm.

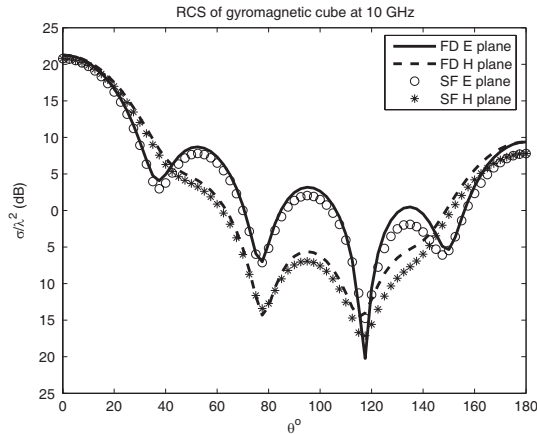**Figure 7.** Incidence of a plane wave on a gyrotropic cube in free space.

As examples, the bistatic RCS calculations of frequency dispersive (FD) and single frequency (SF) computations for 7 GHz and 10 GHz are given in Figures 8 and 9. We again observe a fairly good agreement. We also simulated the structure for 8 and 9 GHz frequencies, but we do not show them here due to limitation of space.

For the gyromagnetic finite cylinder model (Figure 10), the length and the diameter are chosen to be 33.4 mm.

We plotted the single frequency and frequency dispersive RCS calculations for 7 GHz and 10 GHz in Figures 11 and 12. We also modeled and observed good agreement for the simulations at 8 and 9 GHz.
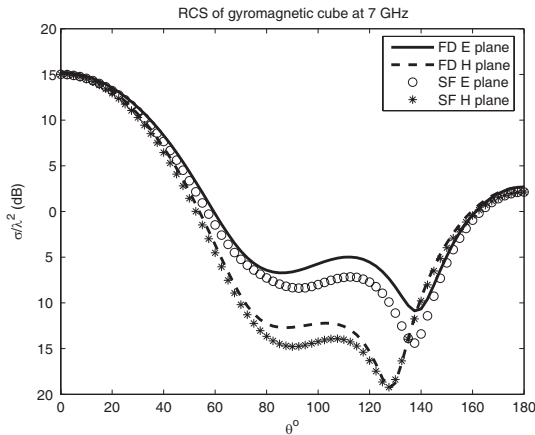


**Figure 8.** The bistatic RCS of frequency dispersive and single frequency simulations of the gyromagnetic cube at 7 GHz.
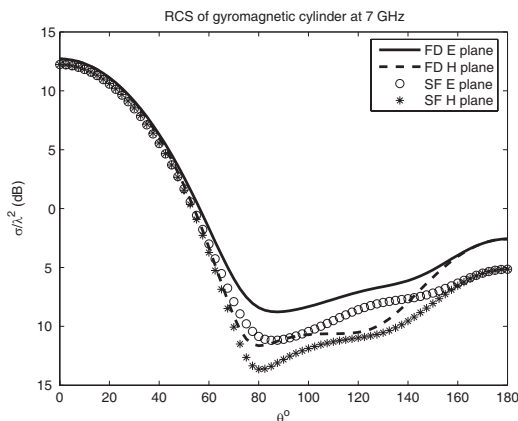
**Figure 9.** The bistatic RCS of frequency dispersive and single frequency simulations of the gyromagnetic cube at 10 GHz.
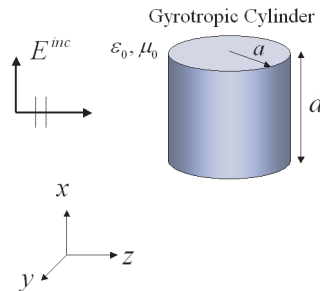


**Figure 10.** Incidence of a plane wave on a gyrotropic cylinder in free space.

As seen from the scattering graphs, the RCS of cube is larger than that of cylinder which is larger than the RCS of sphere. Moreover, as frequency increases, the RCS increases for all three cases.

We do not show the simulation results of 3D frequency dispersive gyroelectric structures, because for every frequency the real component of the diagonal elements of the susceptibility tensors are negative. The single frequency TLM algorithm is unstable for negative real valued diagonal susceptibility tensor elements. But we obtain stable RCS results for frequency dispersive modeling of gyroelectric objects. Nevertheless, we could not find some other data for gyroelectric objects to compare our results.

**Figure 11.** The bistatic RCS of frequency dispersive and single frequency simulations of the gyromagnetic cylinder at 7 GHz.
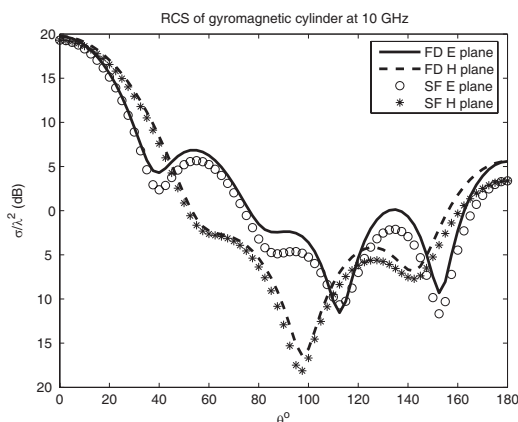


**Figure 12.** The bistatic RCS of frequency dispersive and single frequency simulations of the gyromagnetic cylinder at 10 GHz.

## 4. CONCLUSION

We presented a 3D scattering field TLM algorithm to model frequency dispersive (FD) gyrotropic (gyromagnetic) objects in this paper. We showed the simulation results for three cases — sphere, cube and finite cylinder shaped gyromagnetic objects. The bistatic RCS results of these cases were compared with our single frequency (SF) 3D TLM computations and a fairly good agreement between the simulation results was observed. The material parameters for SF calculations are calculated analytically from the frequency dependent formula

giving the frequency information, whereas the material parameters for FD calculations are discretized in the time domain. Because of this discretization, we observe a little difference between SF and FD results. Finer mesh means making the structures more realistic, because the method uses cubic cells to build the complex shapes. With a finer mesh the sphere model would be more like a sphere or a cylinder would become more like a real cylinder (getting rid of the staircase like structure). This would give more realistic RCS results in our simulations. Better means more realistic. The tensor element values are constant in SF simulation. But in FD, the permittivity and permeability tensor element values are not constant, instead the frequency dependent formulas of these elements are discretized in time domain. Time domain discretization depends on the space discretization in TLM, since the velocity of the wave is constant in the 3D cells of the TLM method (i.e., $\Delta l/\Delta t$ is constant). Due to this discretization, the gyrotropic model in FD simulation behaves similar to the SF model at a given frequency, but not the same. The discrepancies between the SF and FD results originate from this. This modeling method can be used to simulate devices which contain gyrotropic materials, not only in microwave frequencies but also in optical frequency bands.

## REFERENCES

1. Hunsberger, F., R. Luebbers, and K. Kunz, "Finite-difference time-domain analysis of gyrotropic media — I: Magnetized plasma," *IEEE Trans. on Antennas and Propagation*, Vol. 40, No. 12, 1489–1495, 1992.

2. Hunsberger, F. P., "Extension of the finite-difference time-domain method to gyrotropic media," Ph.D. Dissertation, The Pennsylvania State University, 1991.

3. Yaich, M. I., M. Khalladi, I. Zekik, and J. A. Morente, "Modeling of frequency-dependent magnetized plasma in hybrid symmetrical condensed TLM method," *IEEE Microwave and Wireless Components Letters*, Vol. 12, No. 8, 293–295, 2002.

4. Yaich, M. I. and M. Khalladi, "A SCN-TLM Model for the analysis of ferrite media," *IEEE Microwave and Wireless Components Letters*, Vol. 13, No. 6, 217–219, 2003.

5. Paul, J., C. Christopoulos, and D. W. P. Thomas, "Generalized material models in TLM — Part 2: Materials with anisotropic properties," *IEEE Trans. on Antennas and Propagation*, Vol. 47, No. 10, 1535–1542, 1999.

6. Vich, R., *Z Trasform Theory and Applications*, D. Reidel Publishing Company, 1987.

7. Sullivan, D., "Frequency-dependent FDTD methods using *Z* transform," *IEEE Trans. on Antennas and Propagation*, Vol. 40, No. 10, 1223–1230, 1992.

8. Sullivan, D. M., "Nonlinear FDTD formulations using *Z* transforms," *IEEE Trans. on Microwave Theory Tech.*, Vol. 43, No. 3, 676–682, 1995.

9. Sullivan, D., "*Z*-Transform theory and the FDTD method," *IEEE Trans. on Antennas and Propagation*, Vol. 44, No. 1, 28–34, 1996.

10. Huang, Sh. J. and F. Li, "FDTD simulation of electromagnetic propagation in magnetized plasma using *Z* transforms," *International Journal of Infrared and Millimeter Waves*, Vol. 25, No. 5, 815–825, 2004.

11. Paul, J., "Modelling of general electromagnetic material properties in TLM," Ph.D. Dissertation, University of Nottingham, 1998.

12. Yagli, A. F., E. Arvas, and J. K. Lee, "Electromagnetic scattering from three-dimensional gyrotropic objects at single frequency using the TLM method," *ACES Conference*, 642–648, Miami, FL, March 12–16, 2006.

13. Yagli, A. F., J. K. Lee, and E. Arvas, "Monochromatic scattering from three-dimensional gyrotropic bodies using the TLM method," *ACES Journal*, Vol. 22, No. 1, 155–163, 2007.

14. Erkut, H. H., A. F. Yagli, and E. Arvas, "Electromagnetic scattering from a three-dimensional chiral body using the TLM method," *ACES Conference*, 649–654, Miami, FL, March 12–16 2006.

15. Demir, V., "Electromagnetic scattering from three-dimensional chiral objects using the FDTD method," Ph.D. Dissertation, Syracuse University, 2004.

16. Demir, V., A. Z. Elsherbeni, D. Worasawate, and E. Arvas, "A graphical user interface (GUI) for plane wave scattering from a conducting, dielectric or a chiral sphere," *IEEE Antennas and Propagation Magazine*, Vol. 46, No. 5, 94–99, 2004.

17. Soohoo, R. F., *Microwave Magnetics*, Harper & Row Publishers, 1985.

18. Geng, Y. L. and X. B. Wu, "A plane electromagnetic wave scattering by a ferrite sphere," *Journal of Electromagnetic Waves and Applications*, Vol. 18, No. 2, 161–179, 2004.